AIP | Journal of Applied Physics

Third order nonlinear optical susceptibility of Cu:Al2O3 nanocomposites: From spherical nanoparticles to the percolation threshold

R. del Coso, J. Requejo-Isidro, J. Solis, J. Gonzalo, and C. N. Afonso

Citation: J. Appl. Phys. **95**, 2755 (2004); doi: 10.1063/1.1643779
View online: http://dx.doi.org/10.1063/1.1643779
View Table of Contents: http://jap.aip.org/resource/1/JAPIAU/v95/i5
Published by the American Institute of Physics.

Related Articles

Plasmonic reflectors and high-Q nano-cavities based on coupled metal-insulator-metal waveguides
AIP Advances 2, 012145 (2012)

Resonantly enhanced optical nonlinearity in hybrid semiconductor quantum dot–metal nanoparticle structures
Appl. Phys. Lett. 100, 063117 (2012)

Graphene induced tunability of the surface plasmon resonance
Appl. Phys. Lett. 100, 061116 (2012)

Effect of surface plasmon energy matching on the sensing capability of metallic nano-hole arrays
Appl. Phys. Lett. 100, 063110 (2012)

A pancake-shaped nano-aggregate for focusing surface plasmons
J. Appl. Phys. 111, 034308 (2012)

Additional information on J. Appl. Phys.

Journal Homepage: http://jap.aip.org/
Journal Information: http://jap.aip.org/about/about_the_journal
Top downloads: http://jap.aip.org/features/most_downloaded
Information for Authors: http://jap.aip.org/authors

ADVERTISEMENT

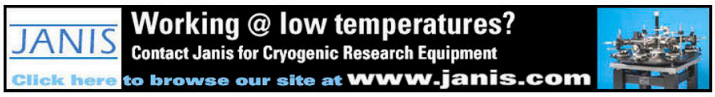

Downloaded 16 Feb 2012 to 161.111.22.69. Redistribution subject to AIP license or copyright; see http://jap.aip.org/about/rights_and_permissions

HTML ABSTRACT + LINKS

Third order nonlinear optical susceptibility of $Cu:Al_2O_3$ nanocomposites: From spherical nanoparticles to the percolation threshold

R. del Coso, J. Requejo-Isidro, J. Solis,[a] J. Gonzalo, and C. N. Afonso
Instituto de Optica, CSIC, Serrano 121, 28006 Madrid, Spain

(Received 1 August 2003; accepted 2 December 2003)

The third order optical susceptibility of metal-dielectric nanocomposite films ($Cu:Al_2O_3$) has been determined by degenerate four wave mixing. The films have been synthesized by alternate pulsed laser deposition and consisted of Cu nanoparticles in an amorphous Al_2O_3 matrix. They have metal volume fractions, p, ranging from 0.07 to 0.45, and morphologies that range from spherical particles (diameter, $\phi \sim 2$ nm) to a random network when close to the percolation threshold. In nanocomposites containing isolated oblate spheroids ($p \leqslant 0.17$), the optical response at wavelengths close to that of the surface plasmon resonance (SPR) can be described in the frame of the Maxwell-Garnett effective medium theory. Above the particle coalescence threshold, in nanocomposites with higher Cu content ($p \geqslant 0.2$), both the linear absorption in the near-infrared and the third order nonlinear optical susceptibility at the SPR are greatly enhanced, the latter achieving values as high as 1.8×10^{-7} esu. These results are discussed in terms of multipolar interactions among particles and giant local resonance effects that appear as a consequence of the particle coalescence and the increase in size of the nanocrystals. © *2004 American Institute of Physics.*
[DOI: 10.1063/1.1643779]

I. INTRODUCTION

The enormous growth of optical communication networks in the past two decades has boosted the research in artificial materials with special optical properties. In particular, devices based on nonlinear optical materials are expected to become important in future high-capacity communication networks through the use of third order optical nonlinearities for ultrafast switching, signal regeneration, and high speed demultiplexing.[1] Artificial materials with large third order optical susceptibility ($\chi^{(3)}$) have thus been an object of increasing interest in recent years.

Third order optical nonlinearities have been studied experimentally in a broad variety of artificial materials that include homogeneous bulk glasses and polymers,[2,3] nano- and mesoscopically structured materials like semiconductor quantum-well structures,[4] and glasses doped with either semiconductor[5] or metal nanocrystals.[6] The existence of local dielectric confinement in the latter type makes the optical response of these nanocomposite materials strongly enhanced at frequencies close to the surface plasmon resonance (SPR) due to collective oscillations of electrons in the metal nanoparticle.

The macroscopic optical properties of nanocomposites are usually described in terms of the volume fraction of metal. Most of the experimental work reported on the optical properties of metal-dielectric nanocomposites has been carried out in the low dilution regime, i.e., for metal volume fractions $p \leqslant 0.01$.[7,8] In this case, the optical response of the nanocomposite can be well described in the framework of the Maxwell–Garnett (MG) effective medium theory[9] and the effective nonlinear third order susceptibility of the composite ($\chi^{(3)}_{\text{eff}}$) can be directly obtained from that of the isolated particles ($\chi^{(3)}_m$).[7,10] In the high concentration regime ($p \geqslant 0.01$), only a few systems have been investigated experimentally, such as Au particles embedded in different matrices[11,12] and Ag colloids with fractal clustering.[13,14] Similarly, only a few theoretical models (see, for instance, Ref. 15 and references quoted therein) have attempted a rigorous description of the optical behavior of metal-dielectric nanocomposites over the whole range of possible metal volume fractions by taking into account the dependence of the local electromagnetic field on the wavelength and the nanostructure of the composite. In spite of this, the properties of composites with high metal volume fractions involving small separations among nanoparticles is of maximum interest because the appearance of multipolar interactions between particles, together with local giant field electromagnetic fluctuations, can significantly enhance different nonlinear optical processes, such as Raman scattering, Kerr refraction, or four wave mixing.[16] In particular, effective third order susceptibilities well above those found in low dilution systems have been predicted in metal-dielectric nanocomposite materials with high metal volume fractions. Their experimental verification is therefore an essential issue for the comprehension of the nonlinearities in artificial structured materials.

The aim of this work is to determine the dependence of the optical properties (linear absorption and third order nonlinear susceptibility) of $Cu:Al_2O_3$ nanocomposites in samples with metal volume fractions ranging from the situation in which Cu is in the form of small spherical particles ($\phi \sim 2$ nm) to the percolation threshold. Copper has been selected for this study because it has been reported to exhibit an intrinsic third order susceptibility in the vicinity of the

[a]Author to whom correspondence should be addressed; electronic mail: j.solis@io.cfmac.csic.es

Downloaded 16 Feb 2012 to 161.111.22.69. Redistribution subject to AIP license or copyright; see http://jap.aip.org/about/rights_and_permissions

TABLE I. Composition of the samples and morphology data including the Cu areal content per nanocomposite layer [Cu] determined by RBS, and the average in-plane diameter (ϕ), height (h) and surface-to-surface separation (S) of the Cu aggregates as determined by GISAXS.

[Cu] (10^{15} at/cm^2/layer)	ϕ (nm)	h (nm)	S (nm)
3.7	1.9	2.2	3.1
5.1	2.7	3.0	3.5
7.7	3.7	3.1	3.4
8.7	4.4	3.4	3.5
9.5	5.1	3.2	3.8
11.5	5.8	3.4	2.6
16	⋯	*3.5*	⋯
21	⋯	*3.9*	⋯

SPR ($\chi_m^{(3)} \sim 10^{-6}$ esu) that is higher than that of Au or Ag,[8,17] making Cu nanocomposites very promising for the development of nonlinear optical devices.

II. EXPERIMENT

The films have been prepared by alternate pulsed laser deposition (PLD) using a pulsed ArF excimer laser ($\lambda = 193$ nm, $f_{rep} = 10$ Hz and $\tau_{FWHM} = 20$ ns) at 2 J/cm^2 to sequentially ablate high purity rotating Al_2O_3 and Cu targets. The films have been grown in vacuum (10^{-6} Torr) on glass substrates held at room temperature. They consist of nanocomposite layers formed by Cu crystalline particles embedded in an amorphous alumina matrix (a-Al_2O_3), alternated with spacing layers of pure a-Al_2O_3 that are approximately 6 nm thick. The layer in contact with the substrate and the last layer both consist of a-Al_2O_3. The films have in total ten nanocomposite layers and the total film thickness is approximately 110 nm.

The areal density of Cu, [Cu], has been determined by Rutherford backscattering spectrometry (RBS) using a 2.0 MeV $^4He^+$ beam, and the morphology of the Cu nanoparticles has been determined by both grazing incidence small-angle x-ray scattering (GISAXS) and high resolution transmission electron microscopy (HRTEM) as reported elsewhere.[18–20] The latter techniques allowed us to determine the average in-plane diameter, height in the direction perpendicular to the film plane, and in-plane surface-to-surface separation among the metal particles. These parameters are summarized in Table I. HRTEM images reported elsewhere[19,20] show that quasispherical particles are formed for the two lower [Cu] value films, whereas the onset of particle coalescence is observed for [Cu] in the $7.7–8.7 \times 10^{15}$(cm$^2 \times$layer) range. Above this coalescence threshold, the particles become elongated in the film plane and can be well described as randomly oriented ellipsoids.[21] For [Cu] $\geqslant 16 \times 10^{15}$(cm$^2 \times$layer) the metal nanocrystals form in-plane filament-like structures and approach the percolation threshold. Under these conditions, it is not possible to determine an average particle height by GISAXS and thus the values included in Table I have been extrapolated from lower [Cu] values assuming a constant volume growth rate.

The linear optical properties of the nanocomposites have been determined from standard reflectivity and transmission measurements made at normal incidence in the 400–800 nm wavelength interval. The characteristic matrix method for determining the reflectivity and transmissivity of a multilayer film[22] together with the refractive index values reported elsewhere for a-Al_2O_3[23] have been used to fit the experimental data to a layered system in order to determine the effective refractive index and the absorption coefficient of the nanocomposite layers.

The modulus of the complex effective third order nonlinear optical susceptibility ($|\chi^{(3)}|$) of the films has been measured by degenerate four wave mixing (DFWM) using the forward folded box configuration.[24] A cavity-dumped, synchronously pumped, mode-locked Rhodamine 6G laser tunable from 575 to 625 nm was used. The laser system provides 12 ps laser pulses with energies about 15 nJ/pulse at a repetition rate that can be selected from single shot up to 41 MHz. The laser beam has been split into three arms, allowing separate control of the delay and polarization of each individual beam. The beams, arranged in a parallel configuration, are then focused and overlapped at the sample surface by using an achromatic 80 mm focal length lens. The beam waist in the focal region of the lens is approximately 30 μm, leading to typical peak power density values around 150 MW/cm^2. The intensity of the conjugated beam produced as a consequence of the nonlinear interaction was then measured as a function of the pump beam intensity by means of silicon photodiodes. The repetition rate used in the experiment was 400 kHz, low enough to avoid cumulative thermal effects between pulses and yet sufficiently high enough to provide a good signal-to-noise ratio when using a standard phase sensitive detection (lock-in) technique at low frequency.

The modulus of the third order nonlinear susceptibility of the nanocomposite material, $|\chi_{eff}^{(3)}|$, has been evaluated using the fit of the cubic dependence of the conjugated signal on the pump intensity with the expression[24]

$$|\chi^{(3)}| = \frac{n^2 c}{32\pi^3} \cdot \frac{\alpha T}{(1-T)\cdot\sqrt{T}} \cdot \sqrt{\frac{I_c}{I_1 \cdot I_2 \cdot I_3}}, \quad (1)$$

where I_j ($j = 1,2,3$) are the intensities of the three incoming beams, I_c is the intensity of the conjugated beam, T is the transmission of the film, and α and n, are respectively, the effective linear absorption and the refractive index of the nanocomposite layers.

As above indicated, the polarization of the different beams could be set independently through half wave plates in order to measure the modulus of the different components of the third order optical nonlinear tensor $|\chi_{ijkl}^{(3)}|$. The resulting values were then compared to the symmetry relations theoretically predicted for centro-symmetric materials. Finally, the temporal evolution of the conjugated signal produced by the films was also measured by using a delay line in one of the three pump beams that are focused onto the sample.

In order to test the reliability of the DFWM experimental setup and the data analysis procedure, we measured the third order nonlinear susceptibility of a 5 mm cell filled with CS_2 (a common reference material). The conjugated intensity ex-

Downloaded 16 Feb 2012 to 161.111.22.69. Redistribution subject to AIP license or copyright; see http://jap.aip.org/about/rights_and_permissions

hibited the expected cubic dependence in the whole pumping power interval studied ($I_0 = 10^7 - 10^8$ W/cm^2). Following the procedure described above, $|\chi^{(3)}_{xxxx}|$ was determined to be $(1.7 \pm 0.3) \times 10^{-12}$ esu that agrees very well with the value commonly accepted in the literature for pumping with picosecond pulses (2×10^{-12} esu).[24] The temporal evolution of the conjugated signal associated with the $\chi^{(3)}_{xxxx}$ component of the susceptibility tensor was found to be consistent with nonlinearity buildup and relaxation times shorter than 2 ps. We have also verified that, within the experimental error, the different components of the nonlinear susceptibility tensor of CS_2 determined in our DFWM experiment fulfill the theoretical relations given elsewhere for axially symmetric orientational effects that dominate the response of CS_2 under picosecond pulses[24]

$$\chi^{(3)}_{xxxx} = \frac{4}{3}\chi^{(3)}_{xyxy} = \frac{4}{3}\chi^{(3)}_{xxyy} = 8\chi^{(3)}_{xyyx}. \quad (2)$$

III. RESULTS

In order to determine the linear and nonlinear optical properties of the Cu:Al_2O_3 nanocomposites from the experimental data, it is necessary to define an effective optical thickness of the nanocomposite layers. Since the metal nanoparticles are the optically active part of the film, the effective thickness of each nanocomposite layer is defined as the average height (h) of the nanocrystals shown in Table I. The total optical thickness of the nanocomposite material is therefore this effective thickness per layer multiplied by the number of nanocomposite layers. Additionally, in order to compare the experimentally determined optical properties of the nanocomposites with the predictions of different theoretical models, the metal volume fraction of the nanocomposite layers has to be determined. This parameter has been calculated through two different methods. The first one calculates the Cu volume fraction (p_{Cu}) assuming that all the Cu is forming the nanoparticles by using the metal areal density per layer and the density of bulk Cu. The second method uses the mean in-plane diameter (ϕ) and height of the nanocrystals to determine first their average volume as $V = \pi\phi^2 h/6$. The volume fraction of the Cu nanoparticles (p_{np}) is then determined as VxN, where N is the areal density of nanoparticles per layer, calculated from their average in-plane center-to-center separation.

Figure 1 shows the volume fractions, p_{Cu} and p_{np}, of nanoparticles in the composite layers as a function of the areal density of Cu deposited per layer determined by both methods. It is clearly seen that both methods lead to a linear behavior, but the volume fraction estimated directly from the metal content is always higher than that calculated from the structural data. Actually, the linear fit of the nanoparticles' volume fraction p_{np} cuts the horizontal axis at an areal density of about 10^{15} at/(cm^2 × layer). This result is not surprising since p_{Cu} considers the whole content of Cu atoms per layer, no matter their state of clustering, while p_{np} is limited by the sensitivity of the structural techniques to the presence of nanoparticles, that is ≈1 nm. The difference between both curves can be thus easily explained if part of the Cu is dissolved in the matrix or forms clusters smaller than 1 nm.

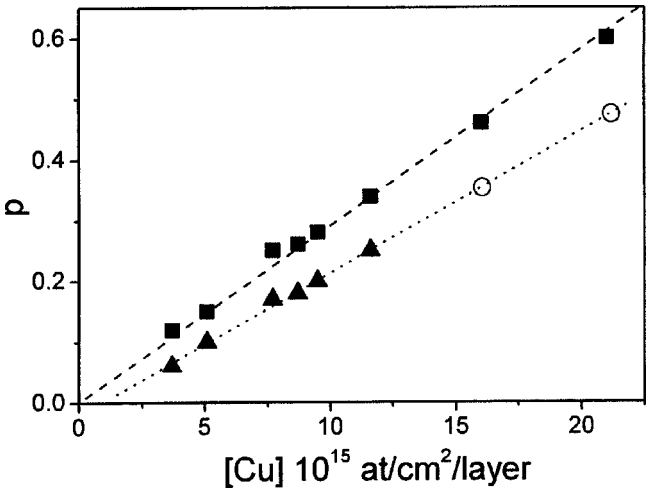

FIG. 1. Cu volume fraction in the nanocomposite layers calculated from, ■: the total Cu content (p_{Cu}), ▲: the volume of the nanoparticles (p_{np}). The dashed lines correspond to best linear fits of each series of data. The values (○) correspond to the volume fraction obtained from the linear fit of p_{np} and have been used for the two samples in which p_{np} is not experimentally accessible.

Figure 2 shows the linear absorption coefficient of four Cu:Al_2O_3 nanocomposites with representative volume fractions as a function of wavelength. The absorption spectra of the sample with the lowest volume fraction ($p_{np} = 0.07$), that is formed by small nanoparticles ($\phi \sim 2$ nm), shows a smooth decrease of the absorption for increasing wavelengths. In contrast, the samples with larger Cu content show a slight decay of the absorption in the 400–550 nm interval which is followed by a broad maximum corresponding to the SPR band around 585 nm. The SPR absorption band shifts to longer wavelengths and becomes broader as the metal volume fraction of the samples increases. For wavelengths beyond the SPR band (~700–800 nm), absorption is enhanced as the metal volume fraction increases. The evolution of the absorption at (a) the SPR ($\lambda = 585$ nm) and (b) in the near IR ($\lambda = 800$ nm) as a function of the volume fraction is presented in Fig. 3 It can be seen that it increases at both wave-

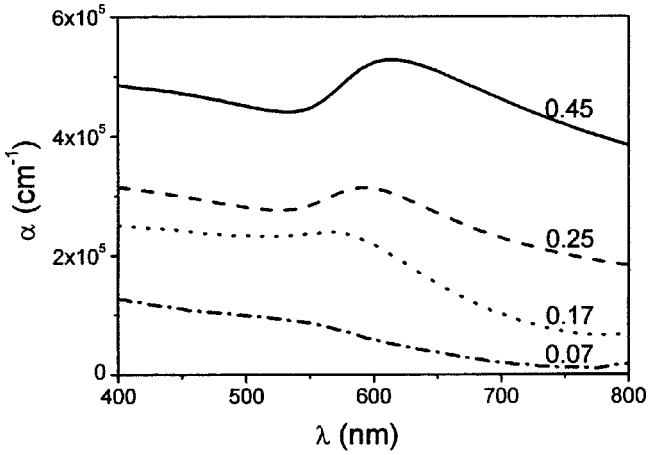

FIG. 2. Absorption coefficient of the Cu:Al_2O_3 nanocomposite layers as a function of wavelength. The curves are labeled by the corresponding volume fraction p_{np}.

Downloaded 16 Feb 2012 to 161.111.22.69. Redistribution subject to AIP license or copyright; see http://jap.aip.org/about/rights_and_permissions

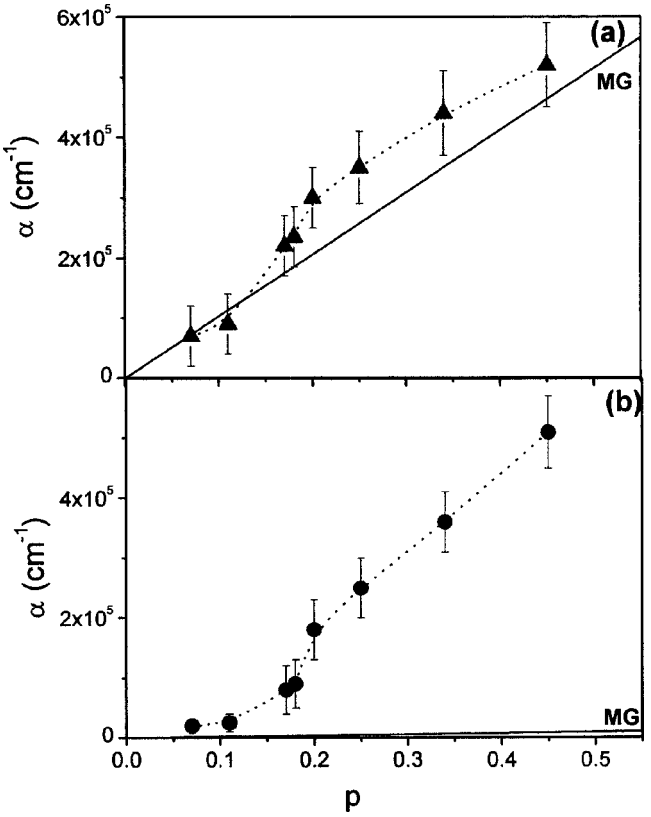

FIG. 3. Linear absorption coefficient of the nanocomposite layers as a function of the metal nanoparticle volume fraction of Cu at (a) 585 nm and (b) 800 nm. The dashed lines are a guide to the eye and the continuous lines correspond to the absorption calculated using the Maxwell–Garnett model.

lengths as p_{np} increases and shows an inflection for p_{np} in the range 0.17–0.2 that is close to the threshold of coalescence among nanoparticles

The linear refractive index of the nanocomposite layers at the SPR has been determined from reflectivity and transmission measurements ($n=2.0\pm0.2$)° along with the value of α. The total effective thickness of the nanocomposite has been used to determine the modulus of the different elements of the third order susceptibility tensor from the DFWM experiments using Eq. (1). The values were consistent in all cases, within the experimental error, with the well known symmetry relations for centro-symmetric materials (Cu has a centro-symmetric crystalline structure and the nanoparticles have no preferential in-plane orientation)[24]

$$\chi^{(3)}_{xxxx}=\chi^{(3)}_{xyxy}+\chi^{(3)}_{xxyy}+\chi^{(3)}_{xyyx}. \tag{3}$$

Since we have measured $\chi^{(3)}(-\omega;\omega,\omega,-\omega)$, the relation for degenerate measurements

$$\chi^{(3)}_{xyxy}=\chi^{(3)}_{xxyy} \tag{4}$$

was also fulfilled in our experiments, and it was checked that, as expected: $\chi^{(3)}_{xyyx}\ll\chi^{(3)}_{xyxy}$.[7] The experimental results show that $|\chi^{(3)}_{xxxx}|$ exhibits a smooth variation (<20%) in the studied wavelength range (575–625 nm) and displays a maximum around 585 nm, in a similar manner to what was observed for the linear absorption. The results presented from now on will thus refer to $|\chi^{(3)}_{xxxx}|$ at 585 nm.

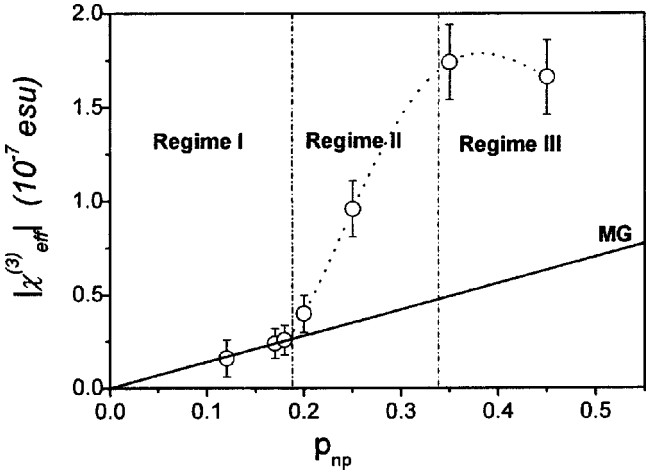

FIG. 4. Modulus of the effective third order susceptibility component $\chi^{(3)}_{xxxx}$ at 585 nm as a function of the volume fraction of Cu nanoparticles. The continuous line is a linear fit of the data with $p<0.20$. The dashed line is a guide to the eye.

Figure 4 shows the evolution of $|\chi^{(3)}_{xxxx}|$ as a function of p_{np}. The specimen having the lowest Cu content ($p_{\mathrm{np}}=0.07$) exhibited a value below our experimental resolution[25] and hence this result has not been plotted. For nanoparticle volume fractions in the interval $0.07<p_{\mathrm{np}}\leqslant0.17$, $|\chi^{(3)}_{xxxx}|$ increases linearly with p_{np}. Above this volume fraction, the effective third order susceptibility undergoes a sharp increase up to a maximum value of 1.8×10^{-7} esu that is achieved for $p_{\mathrm{np}}=0.35$. This is among the highest values ever reported in metal-dielectric nanocomposite materials measured by DFWM with short pulses (<100 ps). For $p_{\mathrm{np}}>0.35$, the nonlinear susceptibility starts to decrease. Since both the linear and nonlinear optical responses plotted in Figs. 3 and 4 exhibit a change of slope for p_{np} values in the range 0.17–0.20, we will refer to the results at either side of this interval as Regimes I ($0\leqslant p_{\mathrm{np}}\leqslant0.17$) and II ($0.2\leqslant p_{\mathrm{np}}<0.35$), respectively. We will refer to the results for $p_{\mathrm{np}}\geqslant0.35$ as Regime III.

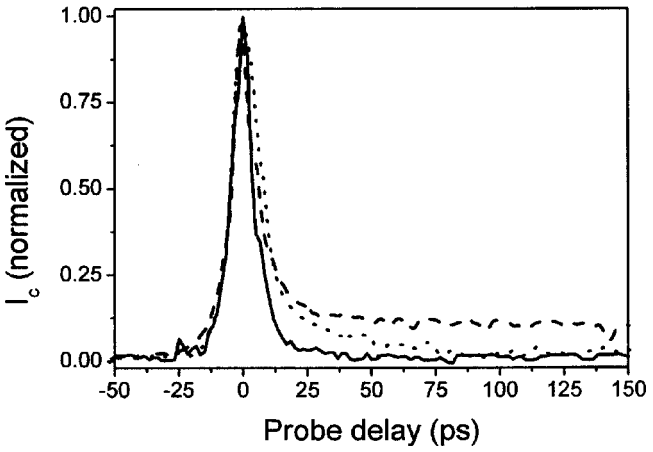

FIG. 5. Time evolution of the conjugated signal associated with $|\chi^{(3)}_{xxxx}|$ in samples with the following metal nanoparticle volume fractions: ——: $p_{\mathrm{np}}=0.25$, · · · ·: $p_{\mathrm{np}}=0.35$, — — —: $p_{\mathrm{np}}=0.45$.

Downloaded 16 Feb 2012 to 161.111.22.69. Redistribution subject to AIP license or copyright; see http://jap.aip.org/about/rights_and_permissions

The time evolution of the conjugated signal associated to eliminate $|\chi^{(3)}_{xxxx}|$ is shown in Fig. 5 for three characteristic temporal behaviors. The time evolution of the conjugated signal for all the samples with a volume fraction $p_{np}<0.35$ is similar, and thus only the data of the temporal response for a representative sample ($p_{np}=0.25$) belonging to Regime II is shown in Fig. 5. This temporal response is identical to the one observed in the CS_2 reference cell, showing buildup and decay times of the conjugated signals shorter than 5 ps and leading to an overall response time shorter than 2 ps after the deconvolution of the pulse shape. For the samples with p_{np} values close or above the percolation limit (Regime III), the buildup time is similar to that observed for lower p_{np} values but the decay of the conjugated signal is slower and exhibits two components. These have been obtained by fitting the experimental data with two exponentials giving a similar fast component $\tau_1=5\pm1$ ps and an additional slow component ($\tau_2=100$ and 450 ps) that increased with the increasing metal volume fraction.

IV. DISCUSSION

Since the nanocomposites in Regime I are the ones in which the nanoparticles are more diluted and have the smaller sizes, we have used the Maxwell–Garnett (MG) model frame in order to fit their linear optical properties. Even though it has been argued that MG theory is only valid for small volume fractions ($p\ll0.1$), it can still be applied to wavelength ranges and nanocomposite structures for which its fundamental assumption (isolated noninteracting particles) is still valid. The absorption coefficient predicted by this model follows a linear dependence with the metal volume fraction[7]

$$\alpha=p\frac{\omega}{nc}|f_{MG}|^2\varepsilon_m'', \tag{5}$$

where ω and c are the frequency and the speed of light, n is linear refractive index of the composite, $f_{MG}=3\varepsilon_d/(\varepsilon_m+2\varepsilon_d)$ is the MG field enhancement factor, and ε_m and ε_d are the complex dielectric function of the metal and the dielectric matrix, respectively. The results achieved with this formulation using for ε_m the value of bulk Cu reported in Ref. 26, are also plotted in Fig. 3 for both the SPR ($\lambda=585$ nm) and near IR ($\lambda=800$ nm) wavelengths. It is seen that the MG prediction agrees well with the experimental results in the neighborhood of the SPR [Fig. 3(a)] for values $p_{np}<0.17$, whereas the experimental values are higher than those predicted by the theory for $p_{np}\geqslant0.2$. This agreement indicates that for particles with sizes between 2 and 4.5 nm (Regime I) the dielectric constant of the metallic nanoparticles (ε_m) is close to that of bulk Cu. Furthermore, the absorption in the IR predicted by MG theory is more than one order of magnitude smaller than that observed even for the lowest p_{np} values.

A general way to describe the relation between the third order nonlinear susceptibility of the nanocomposite $\chi^{(3)}_{eff}$ and the intrinsic susceptibility of the individual nanoparticles $\chi^{(3)}_m$ in the frame of effective medium theories is

$$\chi^{(3)}_{eff}=f_{NL}\cdot\chi^{(3)}_m, \tag{6}$$

where f_{NL} is a nonlinear enhancement factor that depends on the morphology of the nanoparticles and their distribution in the nanocomposite.

In the case of the MG approach, this general formulation turns to[7]

$$\chi^{(3)}_{eff}=p\cdot f_{MG}^2|f_{MG}|^2\cdot\chi^{(3)}_m, \tag{7}$$

where the effective third order nonlinear susceptibility, like the linear absorption, shows a linear dependence with the metal volume fraction. The results achieved in our case using this expression are also plotted in Fig. 4 where it is clearly seen that the MG theory fits the experimental results very well for $p_{np}\leqslant0.17$. Taking into account that the MG model frame (asymmetric in the treatment of the two materials in the composite) has been argued to be valid only for small concentration values ($p\ll0.1$), the fact that both the linear and nonlinear responses of the nanocomposites are well fitted in our case for much larger p values ($p_{np}\leqslant0.17$), suggests that p is not the only parameter controlling the validity of the MG theory.

The slope of the fit of $|\chi^{(3)}_{eff}|$ with the MG theory shown in Fig. 4 has allowed us to calculate $|\chi^{(3)}_m|$ using the values at 590 nm of ε_m for bulk Cu[26] and ε_d for Al_2O_3 films deposited by PLD.[23] The estimated value of $\chi^{(3)}_m=1.5\times10^{-8}$ esu is two orders of magnitude smaller than the values of $\chi^{(3)}_m$ reported in Ref. 8 for Cu nanoparticles in glass. This disagreement can be due to the fact that in Ref. 8 long pulses (7 ns) were used to perform the DFWM experiments and thus the $\chi^{(3)}_m$ data reported are rather related to thermo-optical effects[27] in the matrix. Our experimental conditions featured short pulses (12 ps) and low repetition rates, rendering the measurements insensitive to such spurious effects.

Since MG model predictions show a good agreement with the experimentally determined absorption and nonlinear response near the SPR in Regime I, we can conclude that both ε_m and $\chi^{(3)}_m$ have a negligible size and shape dependence for ϕ between 2 and 4.5 nm. The constant nature of $\chi^{(3)}_m$ within Regime I is compatible with a nonlinearity response mechanism dominated by Fermi smearing (nonequilibrium electron heating), as reported in the case of Au at low concentrations[7] rather than by intraband quantum size effects in which a $1/r^3$ dependence of $\chi^{(3)}_m$ on the particle size would be expected.[7] The discrepancy between the present results and those we reported earlier for Cu nanocomposite films having metal volume fractions within Regime I[28] is most likely related to the conditions in which *Z*-scan experiments were used to determine the nonlinear refractive index (n_2) such that thermo-optical effects[27] may have distorted the values for n_2.

In Regime II, $0.2\leqslant p_{np}<0.35$, both the linear and nonlinear response of the composites depart from the behavior predicted by the MG theory and hence this model can no longer be applied. The other effective medium approximation usually applied for describing the linear and nonlinear optical properties of nanocomposites is the one initially elaborated by Bruggeman and its subsequent extensions.[29,30] Since this approximation treats symmetrically the two com-

Downloaded 16 Feb 2012 to 161.111.22.69. Redistribution subject to AIP license or copyright; see http://jap.aip.org/about/rights_and_permissions

ponents of the composite material, it is expected to be satisfactory for volume fractions higher than the ones considered in the MG theory.[30,31] To calculate the effective nonlinear susceptibility predicted within this approximation, we have used the expression[30]

$$\chi_{\mathrm{eff}}^{(3)}=\frac{1}{p}\cdot\left|\frac{\partial\varepsilon_{\mathrm{eff}}}{\partial\varepsilon_m}\right|\cdot\left(\frac{\partial\varepsilon_{\mathrm{eff}}}{\partial\varepsilon_m}\right)\cdot\chi_m^{(3)}, \tag{8}$$

where $\varepsilon_{\mathrm{eff}}$ is the dielectric constant of Bruggeman's effective medium.[30] At low volume fractions ($p\approx 0.05$), the value of $\chi_{\mathrm{eff}}^{(3)}$ calculated within this approximation [Eq. (8)] is a factor of 2 higher than the value deduced from the MG calculation. For higher volume fractions, $\chi_{\mathrm{eff}}^{(3)}$ shows a saturation value that is nearly independent of p. Although this behavior is in agreement with the calculation performed in Au by Ma, Xiao, and Sheng,[29] it does not agree with the experimental results shown in Fig. 4. Our experimental values show an enhancement of $\chi_{\mathrm{eff}}^{(3)}$ by a factor of 10 when the volume fraction p_{np} increases from 0.1 to 0.35, instead of the factor of 2 derived from Eq. (8). Therefore the initial hypothesis of Bruggeman's model regarding the treatment of the multiple particle interactions and scattering terms[9] is inadequate for describing the nonlinear optical properties of our metal-dielectric nanocomposites. From the above discussion it can be concluded that neither the MG nor the Bruggeman theories describe quantitatively the linear and nonlinear optical properties near the SPR for $p\geqslant 0.2$ and, thus, a different physical framework is thus needed in order to understand the optical response of the nanocomposites within Regimes II and III.

The morphological changes occurring in the nanoparticles for p_{np} in the 0.17–0.20 range can help us pinpoint those factors that are determining the optical response of the nanocomposites at high volume fractions. For the lower p_{np} values (close to 0.1), the metal particles are small and quasispherical nanocrystals. When p_{np} exceeds 0.17, the nanoparticles preferentially grow in the layer plane and become oblate spheroids with their short axis perpendicular to the nanocomposite layer but coalescence is still not significant. In the whole Regime I in which the MG theory is valid, the surface-to-surface separation among particles is >3 nm. Since the MG approximation does not take into account multipolar interactions among neighboring particles, we can conclude that this model is valid for particle separations as short as 3 nm when the particles show dimensions smaller than 4.4 nm. The particle separation limit of 3 nm for neglecting multipolar effects in these $Cu:Al_2O_3$ nanocomposites is similar to the recently reported value of 4.6 nm deduced from the linear optical absorption of Ag nanocomposites.[32] Furthermore, the present results also agree with those reported for Ag nanocomposites in the sense that it is the particle separation, rather than the metal volume fraction or the shape of the particles, that is the essential parameter to be considered when evaluating the importance of multipolar interactions in the optical response.

The enhancement of the nonlinear susceptibility in Regime II occurs once coalescence becomes significant. It is most likely related therefore to the electromagnetic coupling within the coalesced particles that behave as two or more electromagnetically coupled entities. Besides, multipolar scattering effects are known to depend on size (radius, r) and separation (d) of the particles. For the case of spherical particles, a simplified approach shows that the L-order multipolar component of the scattered field scales as $(r/d)^{L+1}$ ($L=2$ for dipoles). Within Regime II, the separation among particles remains approximately constant while their dimensions increase with the Cu content, up to the point where multipolar scattering effects play a crucial role in the optical response of the nanocomposite.

The spectral dependence of the linear absorption gives further support to the importance of multipolar interaction effects among nanoparticles in the optical response of $Cu:Al_2O_3$ composites. The linear absorption for wavelengths longer than that of the SPR departs strongly from that predicted by the MG [as seen in Fig. 3(b)] or Bruggemann models. The MG prediction for the absorption coefficient given by Eq. (5) is based on the dipolar polarizibilities of isolated spheres in the low dilution limit ($p\leqslant 0.1$) and this theoretical approach fails in our case for $p_{\mathrm{np}}\geqslant 0.2$ because of its inability to take into account higher order interaction terms as also reported in Refs. 9 and 33. It has been reported[33–35] that multipolar extinction and multiple particle interactions increase the absorption coefficient of nanocomposites at photon energies lower than that of the SPR[33] and are responsible for the anomalous IR absorption very often observed in metal-dielectric composites.[14] The high linear IR absorption observed in this work is therefore most likely related to multipolar and multiple particle interactions that are not taken into account by MG approximation.

Within Regime III, the nanocomposites are formed by filament-like structures close to the percolation threshold. The third order nonlinear optical susceptibility reaches its maximum value and, for $p=0.45$, it is observed to decrease. This decrease is not surprising since the susceptibility should approach that of bulk Cu, that is orders of magnitude smaller, once the metal forms a continuous layer (or p approaches to 1).

Around the percolation threshold, the presence of multiple particle scattering leads to an enhancement of both the local electric field[36,37] and, accordingly, $\chi_{\mathrm{eff}}^{(3)}$. This effect is overlapped by the presence of a net of metallic filaments, that concentrate the electric field in the point-like edges of the metallic filaments,[38] leading to local giant field enhancement effects of $\chi_{\mathrm{eff}}^{(3)}$ as reported in Ref. 16. Both effects, multiple particle scattering and giant local enhancement, compensate up to some extent the decrease in $\chi_m^{(3)}$ that occurs within the percolated metal structure, giving rise to the wide maximum of $\chi_{\mathrm{eff}}^{(3)}$ observed in Regime III.

From the above description it is clear that the detailed account of the nonlinear response of the composites within Regimes II and III requires theoretical models with a higher degree of complexity than the usual effective medium models. Among them, we can mention the ''granular metal microstructure'' effective medium theory developed in Ref. 29 and the wide theoretical work (and lately also experimental work using near field microscopy[39]) about giant surface-enhanced optical nonlinearities in semicontinuous metal-dielectric films.[15,16] Both theories predict an enhancement of

Downloaded 16 Feb 2012 to 161.111.22.69. Redistribution subject to AIP license or copyright; see http://jap.aip.org/about/rights_and_permissions

the effective third order nonlinear optical susceptibility of several orders of magnitude at high metal volume fractions with the latter in particular predicting the appearance of localized sharp electric fields associated with the localization of surface plasmon modes. As a whole, the most important difference between both models and previous approaches is that they take into account more efficiently the effect of a percolating microstructure and the presence of multiple electromagnetic interactions among nanoparticles.

The time evolution of the conjugated signals shown in Fig. 5, for samples in Regimes I and II is essentially the same as described in Ref. 8 for particles of comparable sizes although for much smaller Cu volume fraction (and thus much longer nanoparticle separations). This indicates that the nonlinear response of our samples should be similarly related to the relaxation of hot electrons from the nonequilibrium state through electron–phonon interactions. The fast electronic buildup and decay times (<2 ps) observed are independent of the nanoparticle size and volume fraction, in spite of the large differences observed in the intensity of both the linear and nonlinear optical responses for specimens with $p_{\mathrm{np}} \leqslant 0.17$ and $p_{\mathrm{np}} \geqslant 0.20$. This result allows us to conclude that multiple particle interactions have no significant influence on the time dependence of the mechanism responsible for $\chi^{(3)}_{\mathrm{eff}}$. Only for volume fractions $p_{\mathrm{np}} \geqslant 0.35$ does the decay of the conjugated signal show two components. The faster one (~ 2 ps) is similar to that observed for lower p_{np} and probably therefore has the same origin. The decay of the slow component (hundreds of ps) depends on the metal volume fraction, being longer the higher the metal volume fraction, and thus it cannot be related to electronic relaxation effects. Its origin is most likely related to the cooling of the metallic lattice by thermal diffusion to the host matrix. This process is more efficient (and faster) for small particles because of their larger surface to volume ratio as already indicated by Bloemer and co-workers in the case of Au nanoparticles.[40] Consequently, the slow component of the decay is slower for those samples closer to the percolation threshold in which the volume of the nanoparticles is larger.

V. CONCLUSION

The comparison between the morphology and the optical properties of Cu:Al_2O_3 nanocomposites shows that for metal contents clearly below the particle coalescence threshold (particle diameters $\leqslant 4.5$ nm and particle surface-to-surface separation $\geqslant 3$ nm), the linear and nonlinear response of the nanocomposites can be well described in the frame of the Maxwell–Garnett effective medium theory. This indicates that the intrinsic optical properties of the metal nanoparticles (ε_m, χ_m) are independent of their size and shape for sizes in the 2–4.5 nm interval. At higher metal contents, the optical response is strongly influenced by the presence of multiple particle interactions and giant local resonance effects that become dominant above the threshold for particle coalescence. These effects give rise to third order susceptibility values in the vicinity of the SPR as high as 1.8×10^{-7} esu for metal contents close to the percolation threshold and to a strong increase of the infrared absorption of the nanocomposites even at much smaller metal contents. The comparison of the behavior of nanocomposites below and above the coalescence threshold suggests that it is the particle separation and size rather than the metal volume fraction that sets the applicability of the Maxwell–Garnett model for describing their behavior, since these parameters fix the relative importance of multiple particle interactions in the optical response of the nanocomposite. For all the morphologies observed, the buildup time of the nonlinearity is very fast (<2 ps) indicating that multiple particle interaction effects have no significant influence on the time dependence of the nonlinear mechanism. Only for samples close to the percolation threshold is the nonlinearity decay time observed to be slower due to thermal relaxation effects.

ACKNOWLEDGMENTS

This work has been partially supported by the Comunidad Autónoma de Madrid (C.A.M. project No. 07T/0038/98), by CICYT (TIC1999-0866) and MCyT (TIC2002-03235). R. d. C. acknowledges financial support of the ''Consejería de Educación de la Comunidad de Madrid'' and the European Social Fund. The authors wish to thank M. Mejías for technical support and Dr. Babonneau (University of Poitiers), Dr. A. K. Petford-Long (University of Oxford), and Dr. D. Hole (University of Sussex) for helpful discussions on the structural and composition data of the studied specimens.

[1] D. Cotter, R. J. Manning, K. J. Blow, A. D. Ellis, A. E. Kelly, D. Nesset, I. D. Phillips, A. J. Poustie, and D. C. Rogers, Science **286**, 1523 (1999).
[2] D. W. Hall, M. A. Newhouse, N. F. Borrelli, W. H. Dumbaugh, and D. L. Weildman, Appl. Phys. Lett. **54**, 1293 (1989).
[3] N. Bloembergen, J. Nonlinear Opt. Phys. Mater. **5**, 1 (1996).
[4] C. J. Hamilton, J. H. Marsh, D. C. Hutchings, J. S. Aitchison, G. T. Kennedy, and W. Sibbett, Appl. Phys. Lett. **68**, 3078 (1996).
[5] G. Banfi, V. Degiorgio, and D. Ricard, Adv. Phys. **47**, 447 (1998).
[6] R. F. Haglund, Jr., C. N. Afonso, G. Battaglin, M. Godbole, F. Gonella, J. D. Hamilton, D. H. Lowndes, R. H. Magruder III, P. Mazzoldi, D. H. Osborne, Jr., and J. Solis, Proc. SPIE **2991**, 90 (1997).
[7] F. Hache, D. Ricard, C. Flytzanis, and U. Kreibig, Appl. Phys. A: Solids Surf. **47**, 347 (1988).
[8] K. Uchida, S. Kaneko, S. Omi, C. Hata, H. Tanji, Y. Asahara, A. J. Ikushima, T. Tokizaki, and A. Nakamura, J. Opt. Soc. Am. B **11**, 1236 (1994).
[9] T. C. Choy, *Effective Medium Theory. Principles and Applications* (Oxford University Press, Oxford, 1999).
[10] E. Sipe and R. W. Boyd, Phys. Rev. A **46**, 1614 (1992).
[11] H. B. Liao, R. F. Xiao, J. S. Fu, P. Yu, G. K. L. Wong, and P. Sheng, Appl. Phys. Lett. **70**, 1 (1997).
[12] H. B. Liao, R. F. Xiao, H. Wang, K. S. Wong, and G. K. L. Wong, Appl. Phys. Lett. **72**, 1817 (1998).
[13] V. Butenko, P. A. Chubakov, Yu. E. Danilova, S. V. Karpov, A. K. Popov, S. G. Rautian, V. P. Safonov, V. V. Slabko, V. M. Shalaev, and M. I. Stockman, Z. Phys. D: At., Mol. Clusters **17**, 283 (1990).
[14] S. Ducourtieux, S. Gresillon, A. C. Boccara, J. C. Rivoal, X. Quelin, P. Gadenne, V. P. Drachev, W. D. Bragg, V. P. Safonov, V. A. Podolskiy, Z. C. Ying, R. L. Armstrong, and V. M. Shalaev, J. Nonlinear Opt. Phys. Mater. **9**, 105 (2000).
[15] A. K. Sarychev and V. M. Shalaev, Phys. Rep. **335**, 275 (2000).
[16] V. M. Shalaev and A. K. Sarychev, Phys. Rev. B **57**, 13265 (1998).
[17] D. Ricard, Ph. Roussignol, and C. Flytzanis, Opt. Lett. **10**, 511 (1985).
[18] R. Serna, C. N. Afonso, J. M. Ballesteros, A. Naudon, D. Babonneau, and A. K. Petford-Long, Appl. Surf. Sci. **138,139**, 1 (1999).
[19] C. N. Afonso, J. Gonzalo, R. Serna, J. C. G. de Sande, C. Ricolleau, C. Grigis, M. Gandais, D. E. Hole, and P. D. Townsend, Appl. Phys. A: Mater. Sci. Process. **69**, S201 (1999).

Downloaded 16 Feb 2012 to 161.111.22.69. Redistribution subject to AIP license or copyright; see http://jap.aip.org/about/rights_and_permissions

[20] R. Serna, J. Gonzalo, A. Suárez-García, C. N. Afonso, J. P. Barnes, A. K. Petford-Long, R. C. Doole, and D. Hole, J. Microsc. **201**, 250 (2001).
[21] R. Serna, C. N. Afonso, C. Ricolleau, Y. Wang, Y. Zheng, M. Gandais, and I. Vickridge, Appl. Phys. A: Mater. Sci. Process. **71**, 583 (2000).
[22] M. Born and E. Wolf, *Principles of Optics* (Pergamon, New York, 1993).
[23] R. Serna, J. C. G. de Sande, J. M. Ballesteros, and C. N. Afonso, J. Appl. Phys. **84**, 4509 (1998).
[24] R. L. Sutherland, *Handbook of Nonlinear Optics* (Dekker, New York, 1996).
[25] The resolution of the DFWM experiment in the present case is about 5×10^{-9} esu. The relatively low resolution is given by the fact that the optically active depth of the sample is only about 30 nm. This makes that only relatively big values of $|\chi^{(3)}_{xxxx}|$ can lead to conjugated signals with intensities above the noise level of the experiment.
[26] E. D. Palik, *Handbook of Optical Constants of Solids* (Academic, San Diego, 1998).
[27] R. de Nalda, R. del Coso, J. M. Requejo-Isidro, J. Olivares, A. Suárez-García, J. Solis, and C. N. Afonso, J. Opt. Soc. Am. B **19**, 289 (2002).
[28] J. M. Ballesteros, J. Solis, R. Serna, and C. N. Afonso, Appl. Phys. Lett. **74**, 2791 (1999).
[29] H. Ma, R. Xiao, and P. Sheng, J. Opt. Soc. Am. B **15**, 1022 (1998).
[30] X. C. Zeng, D. J. Bergman, P. M. Hui, and D. Stroud, Phys. Rev. B **38**, 10970 (1988).
[31] R. J. Gehr, G. L. Fisher, and R. W. Boyd, J. Opt. Soc. Am. B **14**, 2310 (1997).
[32] J. Gonzalo, R. Serna, J. Solis, D. Babonneau, and C. N. Afonso, J. Phys.: Condens. Matter (submitted).
[33] U. Kreibig and M. Vollmer, *Optical Properties of Metal Clusters* (Springer, Berlin, 1995).
[34] D. S. Wang and M. Kerker, Phys. Rev. B **24**, 1777 (1981).
[35] M. Quinten, Appl. Phys. B: Lasers Opt. **73**, 245 (2001).
[36] B. J. Messinger, K. U. von Raben, R. K. Chang, and P. W. Barber, Phys. Rev. B **24**, 649 (1981).
[37] H. Xu, J. Aizpurua, M. Käll, and P. Apell, Phys. Rev. E **62**, 4318 (2000).
[38] P. W. Barber, R. K. Chang, and H. Massoudi, Phys. Rev. B **27**, 7251 (1983).
[39] S. Ducourtieux, V. A. Podolskiy, S. Grésillon, S. Buil, B. Berini, P. Gadenne, A. C. Boccara, J. C. Rivoal, W. D. Bragg, K. Banerjee, V. P. Safonov, V. P. Drachev, Z. C. Ying, A. K. Sarychev, and V. M. Shalaev, Phys. Rev. B **64**, 165403 (2002).
[40] M. J. Bloemer, J. W. Haus, and P. R. Ashley, J. Opt. Soc. Am. B **7**, 790 (1990).

Downloaded 16 Feb 2012 to 161.111.22.69. Redistribution subject to AIP license or copyright; see http://jap.aip.org/about/rights_and_permissions